

# The interaction of $\omega_2$ with the RNA polymerase $\beta'$ subunit functions as an activation to repression switch

Andrea Volante, Begoña Carrasco, Mariangela Tabone and Juan C. Alonso\*

Department of Microbial Biotechnology, Centro Nacional de Biotecnología, CNB-CSIC, 3, Darwin Street, 28049 Madrid, Spain

Received May 12, 2015; Revised July 16, 2015; Accepted July 23, 2015

## ABSTRACT

The  $\omega$  gene is encoded in broad-host range and low-copy plasmids. It is genetically linked to antibiotic resistance genes of the major human pathogens of phylum Firmicutes. The homodimeric forms of  $\omega$  ( $\omega_2$ ) coordinate the plasmid copy number control, faithful partition ( $\omega_2$  and  $\delta_2$ ) and better-than-random segregation ( $\zeta\epsilon\zeta$ ) systems. The promoter ( $P$ ) of the  $\omega\epsilon\zeta$  operon ( $P_\omega$ ) transiently interacts with  $\omega_2$ . Adding  $\delta_2$  facilitates the formation of stable  $\omega_2\cdot P_\omega$  complexes. Here we show that limiting  $\omega_2$  interacts with the N-terminal domain of the  $\beta'$  subunit of the *Bacillus subtilis* RNA polymerase (RNAP- $\sigma^A$ ) vegetative holoenzyme. In this way  $\omega_2$  recruits RNAP- $\sigma^A$  onto  $P_\omega$  DNA. Partial  $P_\omega$  occupancy by  $\omega_2$  increases the rate at which RNAP- $\sigma^A$  complex shifts from its closed (RP<sub>C</sub>) to open (RP<sub>O</sub>) form. This shift increases transcription activation. Adding  $\delta_2$  further increases the rate of  $P_\omega$  transcription initiation, perhaps by stabilizing the  $\omega_2\cdot P_\omega$  complex. In contrast, full operator occupancy by  $\omega_2$  facilitates RP<sub>C</sub> formation, but it blocks RP<sub>O</sub> isomerization and represses  $P_\omega$  utilization. The stimulation and inhibition of RP<sub>O</sub> formation is the mechanism whereby  $\omega_2$  mediates copy number fluctuation and stable plasmid segregation. By this mechanism,  $\omega_2$  also indirectly influences the acquisition of antibiotic resistance genes.

## INTRODUCTION

Resistance to glycopeptides, macrolides, pleuromutilins, phenicols, linezolid and other antibiotics among Gram-positive cocci is generally linked to plasmids whose copy number control, partitioning and post-segregational killing is regulated by the  $\omega$  cassette (1,2). This cassette contains sequences that encode the  $\omega$  or  $\omega_2$  gene products (1). It is thus important to understand how homodimeric  $\omega$  ( $\omega_2$ ) (or  $\omega_2$

[ $\omega_2$ ]) functions, not only because of its intrinsic biological interest, but also because of its relevance to antibiotic resistance transmission (1,2). Plasmids of the *inc18* family are commonly found in *Enterococcus* and *Streptococcus*. These plasmids have a broad host range in Firmicutes. Here,  $\omega$  forms an operon with  $\epsilon$  and  $\zeta$ . Meanwhile,  $\omega_2$  forms an operon with the *ermB* gene (1).

A transcriptional analysis of few *inc18* plasmids (e.g. pSM19035, pIP501 and pAM $\beta$ 1) revealed that  $\omega_2$  controlled the expression of the copy control gene *copS*. Also mediated by  $\omega_2$  was the expression of plasmid partition genes, such as  $\delta$  and  $\omega$ , and toxin-antitoxin systems, such as the  $\omega\epsilon\zeta$  operon (Figure 1A) (1). The *inc18* plasmids persist in the population through a variety of mechanisms controlled by  $\omega_2$ . The  $\omega_2$  protein is a ParB homologue and binds to *parS* centromeres. In concert with  $\delta_2$  (a ParA ATPase),  $\omega_2$  is involved in accurate plasmid partitioning and coupling plasmid replication to faithful segregation (1,3–5). All three *parS* sites (Figure 1A) can cause partition-mediated incompatibility (5). Furthermore, toxin  $\zeta$  stabilizes bacterial plasmids by programming the death of any host cell that fails to inherit a plasmid copy during cell division (1,6). Toxins  $\zeta$  and RelE are the most ubiquitous toxins in nature. In contrast, much less is known about the purpose of the  $\omega_2$  gene product, which is truncated in some members of the family (e.g. pSM19035) (Figure 1A) (1).

*Streptococcus pyogenes* monomeric  $\omega$  (71-residue long, 7.9 kDa) has an unstructured N-terminal domain (NTD, residues 1–24) followed by a ribbon-helix-helix (RHH) fold (residues 25–71). The latter facilitates the formation, in solution, of a dimer that has a pseudo-2-fold symmetry (7–9). The RHH domain recognizes the *parS* centromeres embedded in the promoter regions of the *cop*,  $\delta$ ,  $\omega$  and  $\omega_2$  genes (Figure 1A and Supplementary Figure S1) (4). The operator binding sites are comprised of a series of 6–10 unspaced heptad repeats (5'-T/AATCAC<sup>T</sup>/A-3') in a forward orientation. Alternatively, they consist of two or three repeats of the following: two heptads in a forward orientation followed by one in an inverse orientation ( $\rightarrow\rightarrow\leftarrow$ ) (Supplementary Figure S1). Both the  $\omega_2$  and the NTD lacking  $\omega_2\Delta$ N19 mutant

\*To whom correspondence should be addressed. Tel: +34 91585 4546; Fax: +34 91585 4506; Email: jcalonso@cnb.csic.es

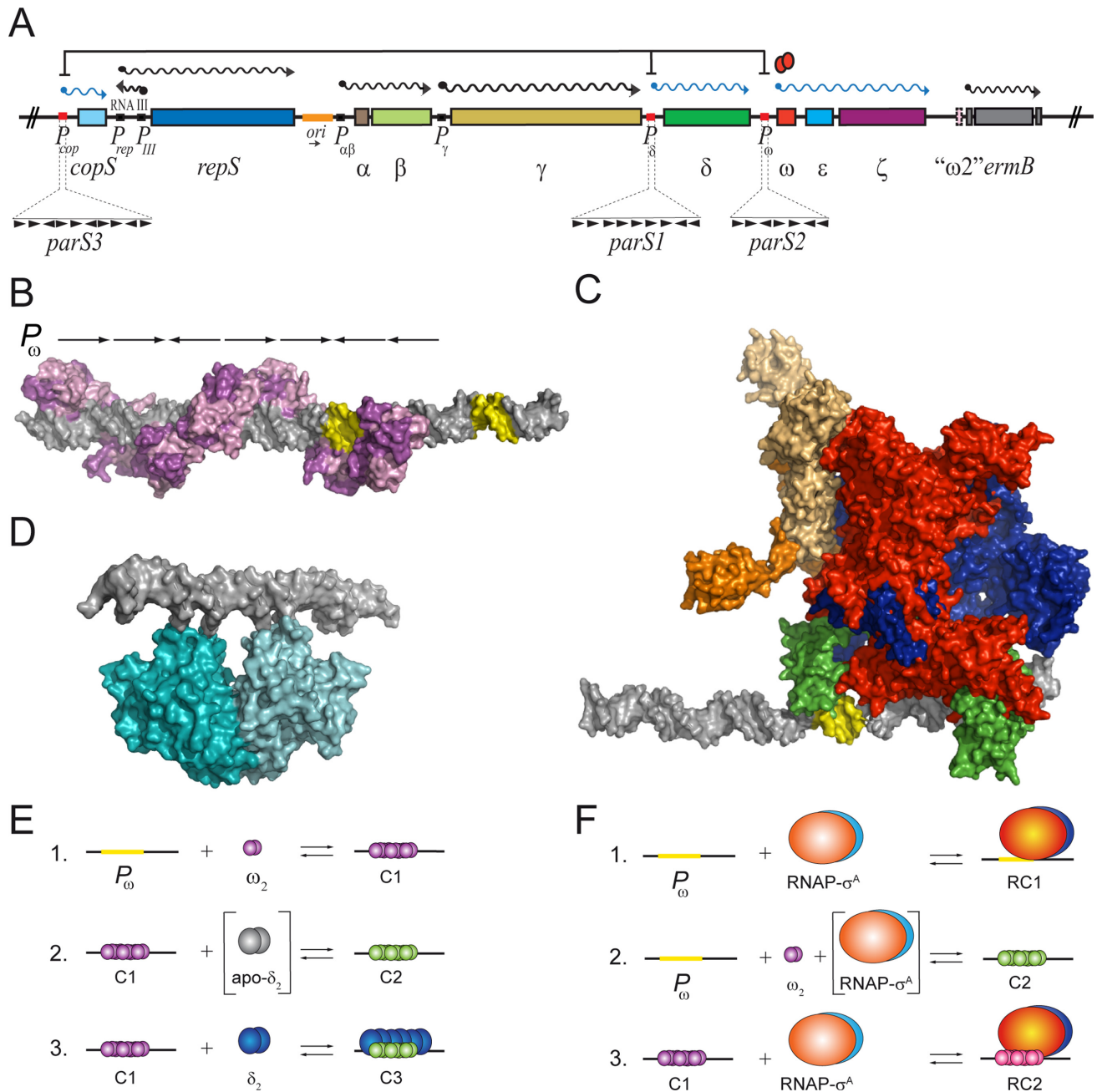


**Figure 1.** Interaction of  $\omega_2$ ,  $\delta_2$  or RNAP- $\sigma^A$  with the  $P_\omega$  operator sites. (A) Genome organization of the relevant region of plasmid pSM19035. The promoters ( $P$ ), the mRNAs and the genes are symbolized by boxes, wavy lanes and rectangles, respectively. The plasmid replication origin (*ori*) is labelled in orange. The direction of replication is denoted by a black arrows below. Protein  $\omega_2$ -mediated transcriptional repression is indicated ( $\omega_2$ , red ovals). The upstream regions of  $P_{copS}$ ,  $P_\delta$  and  $P_\omega$  (red box) which constitute the *cis*-acting *parS* centromeric sites magnified. The  $\omega_2$  cognate sites consist of a variable number of contiguous 7-bp heptad repeats (iterons) symbolized by  $\blacktriangleright$  (in the direct orientation) or  $\blacktriangleleft$  (in the inverted orientation). The number of repeats and their relative orientations are indicated. The genes involved in replication (*copS*, *repS*, RNAIII and  $\gamma$ ), dimer resolution ( $\beta$ ), faithful partition ( $\delta$  and  $\omega$ ), stable segregation ( $\epsilon$  and  $\zeta$ ) are indicated. The antibiotic resistance gene *ermB* and the truncated version of  $\omega_2$  ( $\omega_2^*$ ) are also indicated. (B) A structural model of  $\omega_2$ -bound to  $P_\omega$  DNA which derived from the crystal structure of the complex of the minimal operator site and  $\omega_2\Delta 19$  (PDB ID 1IRQ, 2BNW and 2BNZ). Pink/purple  $\omega_2$  molecules form a left-handed protein-matrix winding around the nearly linear operator DNA. The DNA is represented in grey with the  $-35$  and  $-10$  elements in yellow. (C) Model of RNAP- $\sigma^A$  which is derived from crystal structures of the homologous protein from *T. aquaticus* and *T. thermophilus* (PDB ID 1IW7, 2A6H) together with the  $P_\omega$  DNA from PDB ID 2CAX. Colour coding: brown and light brown refer to  $\alpha_2$ ; blue,  $\beta$ ; red,  $\beta'$  and green,  $\sigma$  subunit. (D) Model of  $\delta_2$  binding to DNA. The atomic coordinates of  $(\delta\text{-ATP}\gamma\text{S}\cdot\text{Mg}^{2+})_2$  were taken from the 2OZE PDB entry. The modelled structures were prepared and visualized with PyMOL version 1.5.0.4. (E) Interactions of  $\omega_2$  and  $\delta_2$  with  $P_\omega$  DNA and each other: 1.  $\omega_2$  (in purple) transiently interacts with  $P_\omega$  DNA forming complex C1; 2. The interaction of  $\omega_2$  with  $\delta_2$ -apo (in grey), leads to functional transition of  $\omega_2$  (in green) and formation of the durable C2 complex; 3. In the presence of ATP,  $\delta_2$  (in blue) binds to C1 to generate C3. (F) Complexes formed by  $\omega_2$  and RNAP- $\sigma^A$  upon binding to  $P_\omega$  DNA: 1. RNAP- $\sigma^A$  bound to  $P_\omega$  DNA forms complex RC1; 2. the interaction of RNAP- $\sigma^A$  with limiting concentrations of  $\omega_2$  leads to a functional transition of  $\omega_2$  and formation of C2; and 3. RNAP- $\sigma^A$  bound to C1 makes RC2.

transiently bind promoters and repress promoter utilization both *in vivo* and *in vitro* (4,9–13).

The minimal  $\omega_2$  binding site is comprised of two contiguous heptads in a forward ( $\rightarrow\rightarrow$ ) or inverted ( $\rightarrow\leftarrow$ ) orientation. It has higher affinity for the latter (see 10). The structure of the complex of  $\omega_2$  bound to  $\rightarrow\rightarrow$  DNA is very similar to the one of  $\omega_2$  bound to  $\rightarrow\leftarrow$  DNA. In neither case does  $\omega_2$  distort the DNA when binding to it (9,14). These structures show that a pair of positively charged antiparallel  $\beta$  strands from  $\omega_2$  insert into the major groove of DNA. The  $\beta$  strands make specific and sequence-dependent contacts with symmetric or asymmetric repetitive sequences that deviate 0.3 Å with respect to the central C-G pair of each repetition (8,9,14). In a full cognate site,  $\omega_2$  is displaced  $\sim 7$ -bp and rotated  $252^\circ$  with respect to its neighbouring dimer. The negatively charged sugar-phosphate DNA backbone faces the positively charged surface of the protein (Figure 1B) (9).

Protein  $\omega_2$  transiently binds with high affinity (apparent dissociation constant [ $K_{Dapp}$ ] =  $5 \pm 1$  nM) and cooperativity to  $P_\omega$  DNA (Figure 1E, condition 1 [C1]) (13). The physical interaction of the apo form of  $\delta_2$  with  $\omega_2$  bound to  $P_\omega$  DNA facilitates a structural transition in  $\omega_2$  that might involve folding of its unstructured NTD (Figure 1E, condition 2) (see 13,15).  $\omega_2$  stably binds  $P_\omega$  DNA with high affinity ( $K_{Dapp}$  =  $0.7 \pm 0.1$  nM), forming the C2 complex ( $\omega_2 \cdot P_\omega$  DNA) (Figure 1E, condition 2). The C2 complex is stable, with a half-life of  $>30$  min, whereas the C1 complex is transient, with half-life of  $<1$  min (10,13,15). However, despite the difference in stability, C1 and C2 have a similar mobility in a PAGE at low protein concentrations.

The  $\delta_2$  protein is a U-shaped ATPase that in its ATP-bound form, binds non-specifically to DNA (Figure 1D) (16). In the presence of ATP,  $\delta_2$  interacts with C1 to form the C3 complex (Figure 1E, condition 3) (13). Since it lacks the unfolded NTD,  $\omega_2\Delta N19$  cannot facilitate C2 and C3 formation (13). Given that  $\delta_2$  (a ParA ATPase) works together with  $\omega_2$  (a ParB centromeric binding protein) bound to *parS* (e.g.  $P_\omega$  DNA) to promote faithful plasmid segregation (12,13), it is likely that  $\delta_2$  also contributes to  $\omega_2$ -mediated transcription regulation.

Transcription initiation by the multisubunit RNA polymerase (RNAP) is an intricate multistep process (17–20). Bacterial RNAP exists in two forms: i) the ubiquitous core enzyme, which consists of the dimeric form of  $\alpha$  ( $\alpha_2$ ), the monomeric form of  $\beta$ ,  $\beta'$ , and one or more of small non-essential subunits; this carries out processive transcription elongation followed by termination; and ii) the RNAP- $\sigma$  holoenzyme, in which a dissociable  $\sigma$  subunit, essential for promoter recognition, has joined the core enzyme (21–23). The *Bacillus subtilis* vegetative RNAP- $\sigma^A$  holoenzyme binds to specific  $-10$  and  $-35$  promoter ( $P$ ) elements to form an unstable closed binary complex (R<sub>P</sub>C) (21,24–27). A RNAP- $\sigma^A$ -assisted isomerization step then occurs. This is mediated by kinetically unstable intermediates (R<sub>P</sub>I). This, in turn, leads to  $P$  melting of  $\sim 14$ -bp ( $-12$  to  $+2$ ) in the DNA surrounding the transcription start site. This process yields the catalytically active, open RNAP- $\sigma^A$ - $P$  DNA complex (R<sub>P</sub>O) (17,28). The structures responsible for the functions associated with R<sub>P</sub>O formation are predominantly located in the  $\sigma$ ,  $\beta$  and  $\beta'$  subunits of the RNAP- $\sigma$  (18,22,23,25,28). In the presence of

nucleotide triphosphates, an initiation complex (R<sub>P</sub>INIT) is formed. This complex is a prerequisite for displacement of RNAP- $\sigma^A$  from the promoter through an elongation complex (R<sub>P</sub>E) (24,25,28). RNAP subunits  $\delta$ ,  $\epsilon$  and  $\omega$  are not essential for this process and their roles are therefore poorly understood.

As a result of the association of regulatory elements to promoter-embedded operator sequences, gene regulation is often achieved at the level of transcription initiation (29). The  $\omega_2$  protein interacts with its cognate sites as a left-handed protein helix wrapped around a nearly linear  $P_\omega$  DNA (9). In this structure the  $-35$  and  $-10$  elements are free to interact with RNAP- $\sigma^A$  (Figure 1B, yellow regions). A model of RNAP- $\sigma$  bound to  $P_\omega$  DNA suggests that  $\omega_2$  might repress transcription by steric hindrance (Figure 1C). However, preliminary results indicate that  $\omega_2$  forms a ternary complex with RNAP- $\sigma^A$  and  $P_{copS}$  DNA (4). These data suggest that  $\omega_2$  regulates transcription through a mechanism that does not exclude the RNAP- $\sigma^A$  from the R<sub>P</sub>C. It is assumed that this mechanism also applies to  $P_\omega$  and  $P_\delta$ . In this study, we aimed to unravel the mechanism of  $\omega_2$ -mediated transcriptional regulation of  $P_\omega$  DNA, *in vitro*, and  $P_\delta$  utilization, *in vivo*. We first characterized the effect that  $\omega_2$  binding to  $P_\omega$  DNA had on RNAP- $\sigma^A$  promoter recognition. We also tested whether or not modifying the stoichiometry of  $\omega_2$ ,  $\delta_2$  and RNAP- $\sigma^A$  resulted in variations in their affinity for  $P_\omega$  DNA. Also investigated was whether or not transcription activation or repression by  $\omega_2$  required direct contacts with RNAP- $\sigma^A$  and  $\delta_2$ . Another important question was whether or not this binding was cooperative. Based on the results of this study, we present a model that explains how  $\omega_2$ -mediated transcriptional regulation functions.

## MATERIALS AND METHODS

### Bacterial strains and plasmids

The *E. coli* strains DH5 $\alpha$  (Invitrogen) and ER2566 (New England Biolabs) and the *B. subtilis* strains BG214, BG508 (4) and NIG2001 (30) were used. The BG508 strain carries  $P_\delta$  fused to a promoter-less *lacZ* gene. This construct was integrated as a unique copy into the *amyE* locus of the *B. subtilis* chromosome (4). In the NIG2001 strain, the wild-type (wt) *rpoC* gene was substituted in the *B. subtilis* genome with a version that had a His-tag coding sequence fused to the 3'-end (30). The  $P_\omega$  bearing pCB30 plasmid was used for promoter analysis, and pHP14 was used for cloning purposes (4). The plasmids used for gene over-expression were pT712 $\omega$  bearing  $\omega$ , pCB746 bearing  $\delta$  (4,11,16), and pT712 $\omega$ D56A bearing the  $\omega$ D56A gene (this work). The single mutations in the  $\omega$  gene were obtained by gene synthesis (Genscript). BG508 cells bearing pHP14 carrying either the  $\omega$ ,  $\delta$ ,  $\omega\delta$ ,  $\omega\Delta N19$ ,  $\omega_2$ ,  $\omega$ K52A,  $\omega$ E53A,  $\omega$ D56A,  $\omega$ R64A or  $\omega$ K70A genes were used for the  $\beta$ -galactosidase assays. The native promoters of these genes were also incorporated into the constructs.

### DNA, RNA, proteins and reagents

Plasmid DNA was purified as described (4). The multiple mutations in heptads 1, 1 plus 2, 7 and 7 plus 6 were ob-

tained by *in vitro* synthesis (Genscript). DNA restriction and modification enzymes and RNaseA were purchased from Boehringer Mannheim and the nucleotides were purchased from Sigma. Gel-purified DNA fragments were end-labelled as described (4). The amount of DNA was quantified using molar extinction coefficient of  $6500 \text{ M}^{-1} \text{ cm}^{-1}$  at 260 nm and was expressed in moles of DNA molecules.

The RNAP- $\sigma^A$  was purified using Ni-NTA and Q-sepharose columns as described (30). The  $\omega_2$  and  $\delta_2$  proteins were purified as described (4,11,16). Protein  $\omega$ D56A was purified as wt  $\omega_2$ . Protein concentrations were calculated using molar extinction coefficients at 280 nm of 2980, 2980, 38 850 and  $236\,000 \text{ M}^{-1} \text{ cm}^{-1}$  for  $\omega_2$ ,  $\omega$ D56A,  $\delta_2$ , and RNAP- $\sigma^A$ , respectively. Concentrations were expressed in molarity of protein monomers for RNAP- $\sigma^A$  and of dimers for  $\delta_2$ ,  $\omega_2$  and  $\omega_2$  derivatives. Note that unless otherwise stated,  $\delta_2$  is in the ATP·Mg $^{2+}$ -bound form.

*B. subtilis* BG508 harbouring different plasmids was grown to  $\text{OD}_{600} = \sim 0.5$  and aliquots were used for  $\beta$ -galactosidase assays (4). The cultures were pelleted and resuspended in buffer B (10 mM  $\text{Na}_2\text{HPO}_4/\text{NaH}_2\text{PO}_4$  pH 7.2, 50 mM  $\beta$ -mercaptoethanol, 1 mM  $\text{MgCl}_2$ , 10 mM KCl) containing 0.4  $\mu\text{g}/\text{ml}$  lysozyme (4). After a 5 min incubation at 37°C, the lysates were clarified by centrifugation for 5 min at 12,000 *g* and assayed for  $\beta$ -galactosidase activity, as described (31).

Protein cross-linking was used to study potential protein-protein interactions. For this, bisdisuccinimidyl suberate (DSS) was employed as the crosslinking agent and SDS-PAGE was used to visualize the result (13). Two-dimensional gel electrophoresis (2D) was performed essentially as described (32). The resolved proteins were transferred onto a 0.45  $\mu\text{m}$  polyvinylidene fluoride membrane (PVDF, Millipore). Rabbit polyclonal anti- $\omega_2$  and anti-RNAP- $\sigma^A$  antibodies were obtained using standard techniques (4).

Far-western blotting was used to probe the direct interaction between  $\omega_2$  and RNAP- $\sigma^A$ . The prey used were  $\omega_2$  (1  $\mu\text{g}$ ), RNAP- $\sigma^A$  (1  $\mu\text{g}$ ) and bovine serum albumin (BSA, 5  $\mu\text{g}$  used as a control); these were resolved by SDS-PAGE and transferred to a PVDF membrane. The protein was re-natured by incubation of the membrane in TBS containing 0.05% Tween, 10% glycerol and 5 mM  $\beta$ -mercaptoethanol followed by a blocking step with 5% skim milk, as described (4). The efficiency of the protein transfer was checked by Ponceau staining. The membrane was then incubated with 2  $\mu\text{g}/\text{ml}$  of bait protein. To detect interactions between the bait and prey, rabbit polyclonal antibodies against the bait were employed as described (33).

Tryptic digestion of gel-purified protein bands, spotting onto the MALDI-targets, and MALDI-TOF-TOF of the spotted peptides were carried out as previously described (34).

### ***In vitro* transcription experiments**

A 423-bp  $P_\omega$  DNA sequence (5 nM) was used as a template for *in vitro* transcription run-off assays. 20  $\mu\text{l}$  reaction mixtures containing 20 nM *B. subtilis* RNAP- $\sigma^A$ , variable concentrations of  $\omega_2$ ,  $\delta_2$  or both, 0.5 mM each of ATP, CTP, GTP and UTP plus 3000 Ci/mmol [ $\alpha$ - $^{32}\text{P}$ ]-UTP in buffer C

(25 mM Tris-HCl, pH 8, 6 mM MgOAc, 5 mM DTT), and 20 U RNasin (Promega) were prepared. After 6 min of incubation at 37°C, the reactions were stopped by adding 10  $\mu\text{l}$  of formamide. RNAs were analysed by 8% denaturing (d) polyacrylamide gel electrophoresis (PAGE), and autoradiographed. Chemical sequencing reactions of the purines were run in parallel to determine the sizes of the cDNAs.

### **Protein-DNA complexes**

For electrophoretic mobility shift assays (EMSA), the 423-bp [ $\alpha$ - $^{32}\text{P}$ ]- $P_\omega$  DNA (0.1 nM) was incubated either with a variety of concentrations of  $\omega_2$ ,  $\delta_2$  or RNAP- $\sigma^A$  or with a constant concentration of one component and a range of concentrations of the others. Incubations were performed in buffer D (50 mM Tris-HCl pH 7.5, 50 mM NaCl, 10 mM  $\text{MgCl}_2$ ) for 15 min at 37°C in a 20  $\mu\text{l}$  reaction. Mixtures were subjected to 6% PAGE in 1xTAE at 4°C. Gels were dried prior to autoradiographical analysis.

In order to obtain  $K_{\text{Dapp}}$  values from the EMSA experiments, the relative concentrations of free DNA and protein-DNA complexes were densitometrically determined under non-saturating conditions using differently exposed autoradiographs of the EMSA gels. The protein concentration needed to trap 50% of the free, labelled DNA containing the same molar concentration of heptads, in complexes is approximately equal to the  $K_{\text{Dapp}}$  under conditions where the DNA concentration is much lower than the  $K_{\text{Dapp}}$ .

Reaction conditions similar to those used for EMSA were employed in footprinting experiments. The 423-bp [ $\alpha$ - $^{32}\text{P}$ ]- $P_\omega$  DNA (1 nM) was incubated with variable protein concentrations and treated with DNaseI, as previously described (4). The samples were resolved by 6% dPAGE and the gel was dried prior to autoradiographical analysis. For  $\text{KMnO}_4$  footprinting, the samples were treated with 1 mM  $\text{KMnO}_4$  for 0.5 min at 37°C, after which the DNA was cleaved with piperidine (35).

## **RESULTS**

### **RNAP- $\sigma^A$ facilitates $\omega_2$ · $P_\omega$ DNA complex formation**

In order to unravel the mechanism of  $\omega_2$ -mediated regulation of  $P_\omega$  utilization, the interaction of  $\omega_2$  and/or RNAP- $\sigma^A$  with  $P_\omega$  DNA was assayed by EMSA (Figure 2A and 2B).  $P_\omega$  DNA has 7 discrete  $\omega_2$  cognate sites. A 423-bp DNA segment containing  $P_\omega$  bound  $\omega_2$  with high affinity to form  $\omega_2$ · $P_\omega$  DNA also known as the C1 complex ( $K_{\text{Dapp}}$  of  $6 \pm 1.7$  nM) (Figure 2C filled circles). When  $P_\omega$  DNA was replaced with a non-specific DNA, the affinity of  $\omega_2$  was low, with a  $K_{\text{Dapp}} > 500$  nM (data not shown) (4). This confirmed previously reported data indicating a high affinity of  $\omega_2$  for  $P_{\text{copS}}$ ,  $P_\delta$  and  $P_\omega$  (10). In addition, binding was found to be cooperative (Figure 2C).  $P_\omega$  also bound RNAP- $\sigma^A$  with high affinity to form RNAP- $\sigma^A$ · $P_\omega$  DNA, also known as the RC1 complex ( $K_{\text{Dapp}}$  of  $29.4 \pm 9$  nM, Figure 2C filled rombs).

In the presence of limiting  $\omega_2$  (0.75 nM) concentrations,  $\omega_2$ · $P_\omega$  DNA complex formation was not observed (Figure 2A, lane 2 and 2C filled circles). Increased concentra-



fixed limiting concentration of RNAP- $\sigma^A$  ( $\sim 4$ -fold below  $K_{Dapp}$ ) and increasing concentrations of  $\omega_2$  were incubated with  $P_\omega$  DNA (Figure 2B, lanes 1–6 and 2C open circles).

To distinguish cooperative binding from a mechanism whereby a protein–protein interaction preceded binding to  $P_\omega$  DNA, the experiment was modified by doubling the concentration of RNAP ( $\sim 2$ -fold below  $K_{Dapp}$ ). In the presence of sub-stoichiometric concentrations of RNAP- $\sigma^A$  (15 nM), the  $\omega_2 \cdot P_\omega$  DNA complex formation became enhanced by at least 10-fold. This resulted in a stoichiometry of  $\sim 2$   $\omega_2/P_\omega$  DNA (Figure 2B, lanes 12–17 and 2C, open circles). This is consistent with the known characteristics of  $\omega_2$  binding to  $P_\omega$  DNA which had a stoichiometry of  $\sim 1 \pm 0.2$   $\omega_2$ /heptad. The minimal  $\omega_2$  binding site consisted of two contiguous heptads (9–12). It is therefore likely that  $\omega_2$  interacts with RNAP- $\sigma^A$ , and that such an interaction induces a conformational change in the former that increases its apparent affinity for  $P_\omega$  DNA. This favours the formation of the C2 complex. Meanwhile, in the absence of RNAP- $\sigma^A$ ,  $\omega_2$ -bound to  $P_\omega$  forms the C1 complex with an 8-fold lower apparent affinity ( $K_{Dapp}$  of  $6 \pm 1.7$  nM).

#### A low concentration of $\omega_2$ facilitates the formation of the RNAP- $\sigma^A \cdot P_\omega$ DNA complex

Limiting concentrations of  $\omega_2$  enhanced the recruitment of RNAP- $\sigma^A$  to  $P_\omega$  DNA (Figure 2B, lanes 1–3 and 12–14). 7.5 nM RNAP- $\sigma^A$  was the limiting concentration of RNAP- $\sigma^A$  necessary to detect the RC2 complex (RNAP- $\sigma^A \cdot P_\omega$  DNA- $\omega_2$ ). This was  $\sim 4$ -fold less than the  $K_{Dapp}$  (Figure 2C open versus filled rombs). It is therefore likely that  $\omega_2$  interacts with RNAP- $\sigma^A$  and facilitates a functional transition of RNAP- $\sigma^A$ . To test whether or not  $\omega_2$  and RNAP- $\sigma^A$  co-localize in a RC2 complex,  $\omega_2$  and RNAP- $\sigma^A$  were incubated with  $P_\omega$  DNA and subjected to DNase I footprinting analysis. The  $\omega_2$  protein protected nucleotides –22 to –75 (with a numbering relative to the +1 transcription start site) (Supplementary Figure S2A, lanes 4–5). Meanwhile, RNAP- $\sigma^A$  made a weak but significant contact with a segment located between positions –53 to +18. In parallel, a clearly hypersensitive site appeared at position –37. This is denoted by a dotted line square in Supplementary Figure S2A, lanes 6–9. Addition of a limiting concentration of  $\omega_2$  of  $\sim 4$ -fold below the  $K_{Dapp}$  resulted in the disappearance of the hypersensitive site. This effect was reversed upon increasing the concentration of RNAP- $\sigma^A$  (Supplementary Figure S2A, lanes 10–13). It was also reversed by increasing the concentration of  $\omega_2$  to  $\sim 2$ -fold below the  $K_{Dapp}$  (Supplementary Figure S2B, lanes 13–16). Judging by the fading out of the hypersensitive site at position –37, it is likely that limiting concentrations of  $\omega_2$  or RNAP- $\sigma^A$  reposition RNAP- $\sigma^A$  on the  $P_\omega$  DNA.

Addition of sub- to stoichiometric concentrations of  $\omega_2$  led to an increase in the formation of RC2 (RNAP- $\sigma^A \cdot P_\omega$  DNA- $\omega_2$ ) complex formation by at least 3-fold ( $K_{Dapp}$  of  $9.5 \pm 3.4$  nM) (Figure 2B, lane 17 and 2C, open rombs). Equilibrium was thus reached at about  $\sim 4$   $\omega_2$ /RNAP- $\sigma^A/P_\omega$  DNA. These results suggested that there was not a sufficient number of  $\omega_2$  molecules to occupy the seven  $P_\omega$  heptads. Since  $\omega_2$  binds with a slightly higher affinity and cooperativity to heptad pairs in the  $\rightarrow \leftarrow$  than in the  $\rightarrow \rightarrow$  orienta-

tion (10), we favour the hypothesis that the  $\rightarrow \leftarrow$  heptads at positions –41 to –27, which overlap the –35 element and its neighbours, might be the ones recruited by  $\omega_2$  to interact with RNAP- $\sigma^A$ . Indeed, sub- to stoichiometric concentrations of  $\omega_2$  bound to  $P_\omega$  DNA protected this region from DNase I attack (Supplementary Figure S2B, lanes 3–6). Meanwhile at stoichiometric concentrations RNAP- $\sigma^A$  made weak but extensive contacts with the upstream region, which had the same exposed hypersensitive site at position –37 (Supplementary Figure S2B, lanes 8–11). At sub-stoichiometric concentrations of  $\omega_2$ , RNAP- $\sigma^A$  made extensive contacts with the upstream –35 region. The hypersensitive site at position –37 remained exposed (Supplementary Figure S2B, lanes 13–16). This hypersensitive site was lost in the presence of stoichiometric concentrations of  $\omega_2$ . Meanwhile, protection from DNase I was only observed in a stretch of DNA between positions –72 to –21 (Supplementary Figure S2B, lanes 18–21). In light of these results, it is likely that: (i)  $\omega_2$  physically interacts with RNAP- $\sigma^A$ ; and (ii) depending on the experimental conditions,  $\omega_2$  either displaces RNAP- $\sigma^A$  from or re-localises with it on  $P_\omega$  DNA.

#### The interaction between $\omega_2$ and $\delta_2$ does not affect RNAP- $\sigma^A$ binding to $P_\omega$ DNA

Protein  $\delta_2$  bound non-specific DNA ( $K_{Dapp}$   $130 \pm 20$  nM) in the presence of ATP. This led to the formation of the DC complex (Supplementary Figure S3A, lanes 6–8) (13). Binding of  $\delta_2$  to non-specific DNA increased 3 to 4-fold in the presence of  $\omega_2 \cdot P_\omega$  DNA (Supplementary Figure S3A, lanes 10–12, and S3C, empty squares). In the absence of ATP,  $\delta_2$  only augmented the affinity of  $\omega_2$  for  $P_\omega$  DNA by 6- to 10-fold (C2 formation) (Supplementary Figure S3B, lanes 10–15 and Figure 1E, condition 2). This was consistent with observations that: (i) the presence of apo- $\delta_2$  decreased the off rate of  $\omega_2$  from  $\omega_2 \cdot P_\omega$  DNA complexes; (ii) the presence of  $\omega_2$  significantly increased the half-life of the  $\delta_2 \cdot P_\omega$  DNA complexes in the presence of ATP (13); and (iii) upon interacting with  $\delta_2$ ,  $\omega_2$  that is bound to  $P_\omega$  DNA (*parS*) undergoes a structural transition that might involve the formation of an  $\alpha$ -helix in the normally unstructured NTD (see 15).

To test whether the interaction of  $\omega_2$  with  $\delta_2$  or RNAP- $\sigma^A$  are mutually exclusive or if the interaction between  $\delta_2$  and  $\omega_2$  affects  $\omega_2$ -mediated recruitment onto the  $P_\omega$  DNA of RNAP- $\sigma^A$ , limiting concentrations of  $\omega_2$  ( $\sim 8$ -fold below  $K_{Dapp}$ ) and/or RNAP- $\sigma^A$  ( $\sim 4$ -fold below  $K_{Dapp}$ ) were incubated with increasing  $\delta_2$  concentrations and subjected to an EMSA (Supplementary Figure S3A and S3B, lanes 10–15). In the presence of ATP, assembly of the ternary C3 complex ( $\delta_2 \cdot \omega_2 \cdot P_\omega$  DNA) occurred (Supplementary Figure S3A, lanes 10–15). However, these results were not observed when ATP was omitted (Supplementary Figure S3B, lanes 10–15). Meanwhile, assembly of the ternary RC2 complex ( $\omega_2 \cdot P_\omega \cdot$  RNAP- $\sigma^A$ ) was observed without ATP (Supplementary Figure S3A and S3B, lanes 13–15). Finally, in the presence of ATP,  $\delta_2$  did not significantly affect the affinity of RNAP- $\sigma^A$  for  $P_\omega$  in the presence of ATP (Supplementary Figure S3D, lanes 8–16).

### Whether $\omega_2$ functions as an activator or repressor is dependent on its concentration

Protein  $\omega_2$  binds  $P_{copS}$ ,  $P_\delta$  and  $P_\omega$  DNA with a stoichiometry of  $\sim 1 \pm 0.2 \omega_2$  /heptad (9,12). We previously mapped the pSM19035 transcription start sites of  $P_{copS}$ ,  $P_\delta$  and  $P_\omega$  (see Supplementary Figure S1). In that study, we showed that  $7.5 - 15 \omega_2/P_{copS}$ ,  $P_\delta$  or  $P_\omega$  DNA represses promoter utilization (4). To gain insight into the mechanism by which  $\omega_2$  regulates promoter utilization, we performed transcription run-off experiments using RNAP- $\sigma^A$  (at  $K_{Dapp}$ ) in the presence of increasing concentrations of  $\omega_2$ . Linear  $P_\omega$  DNA containing seven heptads was used as the template (Figure 3A). As expected, 282-nt mRNA transcripts were produced (Figure 3B, lane 1). This result is consistent with the location of the initial nucleotides of  $P_\omega$ , which had been previously mapped *in vivo* (4).

In the presence of limiting concentrations of  $\omega_2$  (0.9 and  $1.8 \omega_2/P_\omega$  DNA), transcriptional activation was modest (1.4- to 1.7-fold), but reproducible (Figure 3B, lanes 2–4, and 3C). Protein  $\omega_2$  might preferentially bind the heptads of the  $P_\omega$  DNA overlapping the  $-35$  element. To test this hypothesis, the heptad 7, heptads 6 plus 7 and, as controls, heptads 1 or 1 plus 2 were inactivated (Figure 3A). As documented in Supplemental material Annex 1, the selective occupancy of heptads 6 and 7 versus 1 and 2 plays a minor role, if at all, in  $\omega_2$ -mediated activation of  $P_\omega$  utilization.

Stoichiometric concentrations of  $7.5 \omega_2/P_\omega$  DNA inhibited  $P_\omega$  expression by 4- to 8-fold. At slightly saturating conditions ( $15 \omega_2/P_\omega$  DNA or  $\sim 2 \omega_2$ /heptad) mRNA synthesis halted completely ( $>50$ -fold) (Figure 3B, lanes 5 and 6). Concentrations of  $\omega_2$  equal to or higher than those required to repress  $P_\omega$  did not affect the expression of the unrelated promoter ( $P_{cro}$  of phage A2) (data not shown). We could hence rule out RNase contamination or any other non-specific effect as the reason for the lack of RNA synthesis. It is therefore likely that  $\omega_2$  has a dual activity: at limiting concentrations it facilitates the  $P_\omega$ -RNAP- $\sigma^A$  interaction, but at stoichiometric concentrations and higher, transcriptional repression results.

### Limiting concentrations of $\omega_2$ facilitate the transition from $RP_C$ to $RP_O$ and stoichiometric concentrations of $\omega_2$ block this shift

To discern the mechanism of  $\omega_2$ -mediated repression of  $P_\omega$ , we investigated  $RP_O$  complex formation and abortive initiation ( $RP_{INIT}$ ) effects in the presence of variable concentrations of  $\omega_2$ . For this, we carried out  $KMnO_4$  footprinting assays in the presence or absence of GTP and ATP. Up to 9-nt long transcripts were synthesized in these assays (see Supplementary Figure S1).

No oxidized thymines were detected on the template strand after 50 s of  $KMnO_4$  exposure (Figure 4, lanes 1, 7, 13 and 19). In the absence of nucleotide precursors, the position in the  $P_\omega$  DNA of non-base-paired thymines preferentially attacked by  $KMnO_4$  revealed that RNAP- $\sigma^A$  promoted spontaneous formation of a  $RP_O$  complex centred at position  $-11T$  and  $-10T$  of the template strand, rather than an extended  $P$  melting of  $\sim 14$ -bp (from  $-12$  to  $+2$ ) (Figure 4, lanes 2 and 8).  $KMnO_4$ -promoted cleavage of

RNAP- $\sigma^A$  bound template increased in the presence of sub-stoichiometric concentrations of  $\omega_2$  (Figure 4, Supplementary Figure S4A, lanes 3–4). Cleavage was inhibited at saturating concentrations of  $\omega_2$  (Figure 4, Supplementary Figure S4A, lanes 5–6). However, increased cleavage was not observed when sub-stoichiometric  $\omega_2$  concentrations were added to reactions containing RNAP- $\sigma^A$ , i.e. with a preformed  $RP_O$  (Figure 4, lanes 9–10).

In the presence of ATP and GTP, RNAP- $\sigma^A$  promoted abortive initiation and synthesis of up to 9-nt oligonucleotides ( $RP_{INIT}$ ) (data not shown).  $KMnO_4$  attack revealed the formation of an extended single-stranded bubble that cleaved at positions  $-10T$ ,  $-6T$ ,  $-5T$  and  $+7T$  (Figure 4, lanes 14 and 20). When  $\omega_2$  and RNAP- $\sigma^A$  were left out, no cleavage was observed (Figure 4, lanes 13 and 19). Pre-incubation of  $P_\omega$  DNA with sub-saturating concentrations of  $\omega_2$  followed by addition of RNAP- $\sigma^A$  resulted in a significant increase ( $\sim 2.5$ -fold) in  $KMnO_4$  cleavage (Figure 4, lane 15 and 21 and Supplementary Figure S4B). At higher  $\omega_2$  concentrations, the reaction became inhibited (Figure 4, lanes 17–18, Supplementary Figure S4A, lanes 15–16 and S4B). However, RNAP- $\sigma^A$ -mediated  $RP_O$  formation was hardly, if at all, affected by addition of  $\omega_2$  to the preformed RNAP- $\sigma^A$ - $P_\omega$  complexes (Figure 4, lanes 21–24).

Altogether, these data suggest that: (i)  $\omega_2$  does not repress transcription by sterically hindering the interaction between RNAP- $\sigma^A$  and  $P_\omega$  DNA; (ii) in the absence of the nucleotides cofactors, RNAP- $\sigma^A$  forms a short  $RP_O$  complex on  $P_\omega$  centred at position  $-11T$  and  $-10T$ ; (iii) limiting concentrations of  $\omega_2$  push  $RP_O$  to begin RNA synthesis ( $RP_{INIT}$ ); (iv) stoichiometric concentrations of  $\omega_2$  inhibit  $RP_O$  formation, with  $\omega_2$  blocking the isomerization of  $RP_C$  to  $RP_O$ ; and (v)  $\omega_2$  has no apparent effect on pre-formed  $RP_O$ . We cannot rule out that saturating concentrations of  $\omega_2$  may inhibit transcription by steric occlusion or relocation of RNAP- $\sigma^A$  on preformed  $\omega_2$ - $P_\omega$  complexes (see Supplementary Figure S2B, lanes 18–21).

### Protein $\delta_2$ represses $P_\omega$ expression

In the presence of ATP,  $\delta_2$  binds non-specific DNA with a  $K_{Dapp} = 130 \pm 20$  nM (Supplementary Figure S3A, lanes 6–8) (13). As shown in Figure 3B (lane 1 versus 7–10), limiting concentrations of  $\delta_2$  did not affect transcription of  $P_\omega$ . Meanwhile, stoichiometric and saturating concentrations of  $\delta_2$  inhibited  $P_\omega$  utilization (2.8- to 3.5-fold). Ultimately utilization was blocked entirely.

To unravel the mechanism of  $\delta_2$ -mediated  $P_\omega$  repression,  $KMnO_4$  cleavage experiments were performed. Pre-incubation of  $P_\omega$  DNA with sub-stoichiometric to stoichiometric concentrations of  $\delta_2$  followed by addition of RNAP- $\sigma^A$  did not alter the pattern of  $KMnO_4$  cleavage obtained in the absence of  $\delta_2$  (Supplementary Figure S5, lanes 1–4 versus 5). This result suggested that  $\delta_2$  represses  $P_\omega$  (Figure 3, lanes 9–10) through gene silencing, i.e. halting RNAP elongation (Figure 3, lanes 9–10). The same model has been as proposed for other ParAB systems to which  $\delta_2$  and  $\omega_2$  belong (36,37). This model is also consistent with the observation that non-specific binding of  $\delta_2$  to DNA might occlude RNAP- $\sigma^A$  clearance or affect RNAP mediated elongation.

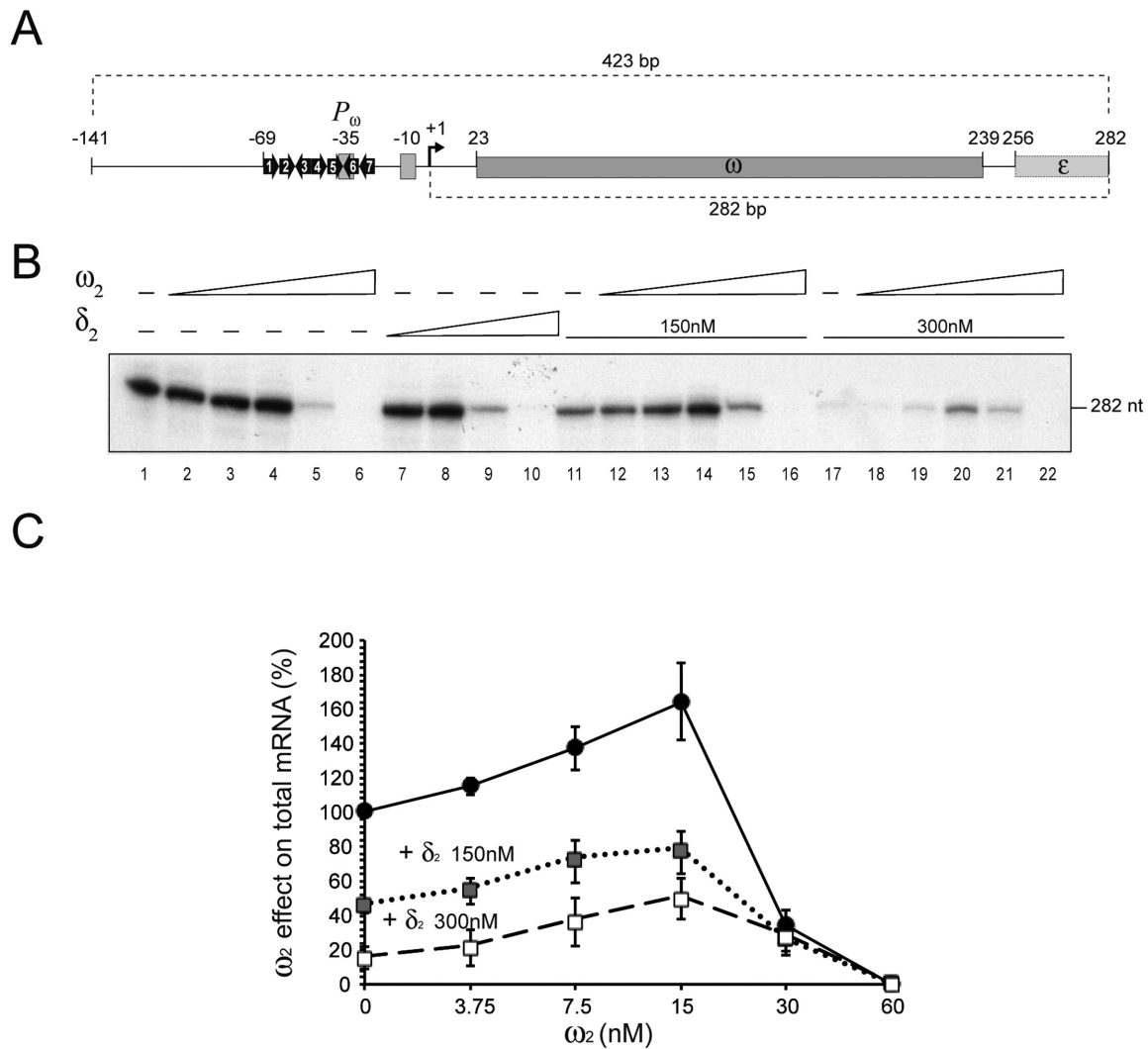


**Figure 3.** RNAP- $\sigma^A$  mediated transcription as a function of the presence or absence of  $\omega_2$  and  $\delta_2$ . (A) A 423-bp DNA segment containing  $P_\omega$  is depicted. The heptads are labelled and their relative orientations are represented by arrows. The positions of the  $-35$  and  $-10$  elements are indicated with filled rectangles. The transcription start site is represented with a solid arrow bent  $90^\circ$ . The  $\omega$  and part of the  $\epsilon$  gene are indicated as well. (B) Run-off experiments: the 423-bp  $P_\omega$  DNA (5 nM) was the template in an *in vitro* transcription experiment using [ $\alpha^{32}\text{P}$ ]-UTP in buffer C. RNAP- $\sigma^A$  (20 nM) was present in all cases. Results shown for transcription in the absence (lane 1) or presence of increasing concentrations of either  $\omega_2$  (3.7, 7.5, 15, 30 and 60 nM, lanes 2–6) or  $\delta_2$  (37, 75, 150, 300 nM, lanes 7–10). Also shown are results of assays in the presence of either 150 or 300 nM  $\delta_2$  (lanes 11–16 or 17–22 respectively) with increasing concentrations of  $\omega_2$ . (C) Quantification of mRNA synthesis in the presence of increasing concentrations  $\omega_2$  alone or in the presence of a fixed concentration of  $\delta_2$  (150 or 300 nM). Shown here are the analysed results from five independent experiments.

### Protein $\delta_2$ acts as a co-activator of $P_\omega$ expression

Upon coming into contact with  $\omega_2 \cdot P_\omega$  complexes,  $\delta_2$  protein bound to non-specific DNA relocates onto  $\omega_2 \cdot P_\omega$  to form ternary C3 complexes (Figure 1E, condition 3) (12). The C3 complex is characterized by a longer half-life than is C1 ( $\omega_2 \cdot P_\omega$  DNA). To test whether C3 might affect transcription,  $P_\omega$  run-off experiments were performed (Figure 3B, lanes 11–22). At 150 nM, a concentration of  $\delta_2$  equivalent to its  $K_{Dapp}$ , addition of limiting concentrations of  $\omega_2$  (1.8 to 3.7  $\omega_2/P_\omega$  DNA) significantly stimulated mRNA synthesis by  $>3$ -fold (Figure 3B, lanes 12–14 and 3C). Nevertheless, synthesis was attenuated and ultimately blocked at higher concentrations of  $\omega_2$  (Figure 3B, lanes 15–16).

At 300 nM,  $\delta_2$  significantly reduced  $P_\omega$  utilization by  $\sim 14$ -fold (Figure 3B, lanes 1 versus 17). Addition of lim-

iting concentrations of  $\omega_2$  (1.8–3.7  $\omega_2/P_\omega$  DNA or 0.2–0.5  $\omega_2$ /heptad) significantly stimulated  $P_\omega$  dependent mRNA synthesis by  $>6$ -fold (Figure 3B, lanes 18–20, and 3C). As expected,  $\omega_2$  blocked  $P_\omega$  utilization when used at the slightly saturating concentrations of 15  $\omega_2/P_\omega$  DNA (Figure 3B, lane 22). It is likely, therefore, that whether  $\omega_2$  acts as a transcriptional activator or a repressor hinges on its concentration (Figure 3C). Moreover, while by itself repressing  $P_\omega$  utilization,  $\delta_2$  apparently behaves as a transcriptional co-activator. This is consistent with the observations that: i) the half-life of  $\omega_2 \cdot P_\omega$  complex increased  $\sim 30$ -fold in the presence of  $\delta_2$  (10,13); and ii) upon interacting with  $\delta_2$ ,  $\omega_2$  bound to  $P_\omega$  DNA, a rearrangement of its unstructured NTD occurs (see 15).



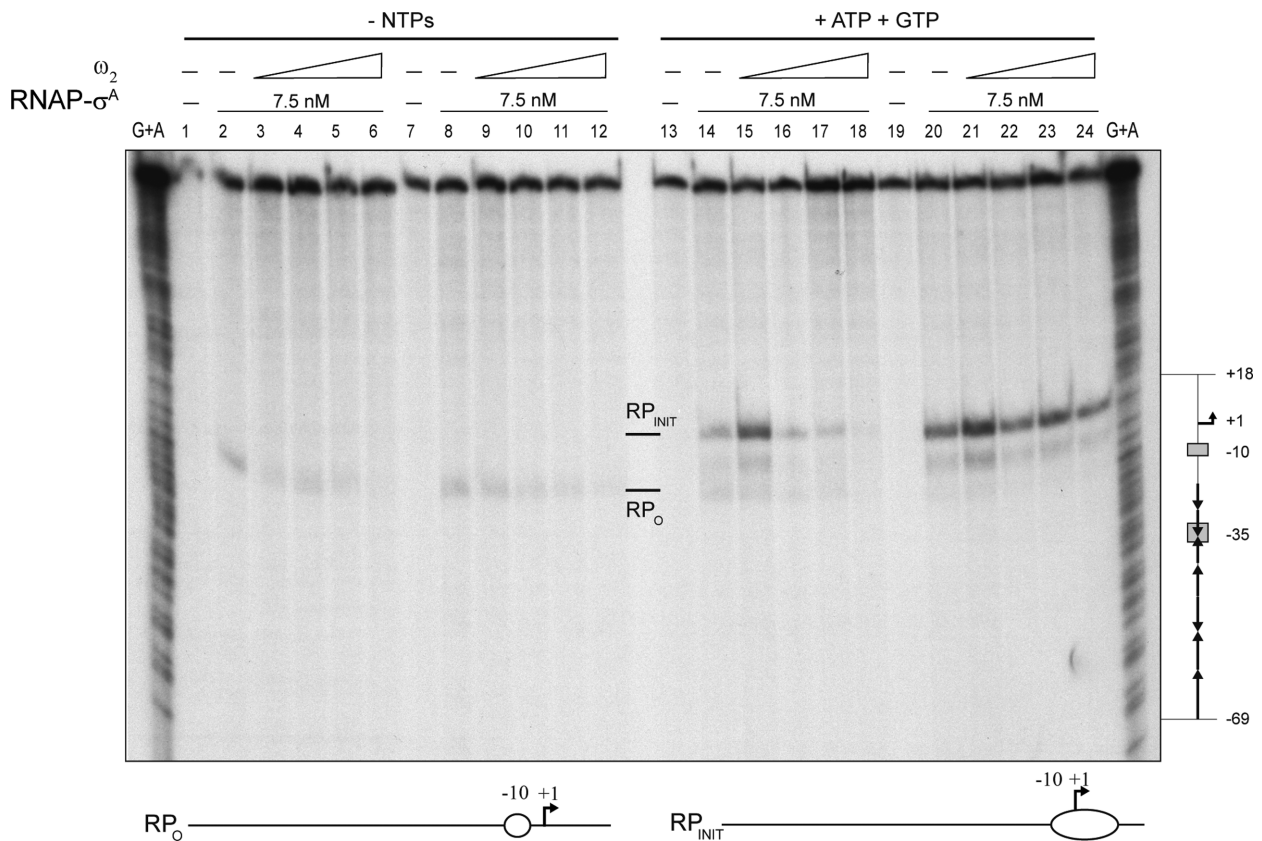


**Figure 4.** Effect of  $\omega_2$  on the formation of  $RP_0$  at  $P_{\omega}$ . The 423-bp [ $\alpha^{32}P$ ]- $P_{\omega}$  DNA (1 nM) was pre-incubated with increasing concentrations of  $\omega_2$  (7.5, 15, 30 and 60 nM; lanes 2–6 and 14–18) or with 7.5 nM  $RNAP-\sigma^A$  (lanes 8–12 and 20–24) in buffer C. A second protein was added along with the initiating nucleotides, GTP and ATP (as indicated). DNA melting was probed by  $KMnO_4$  footprinting as a way of observing the open complex. The positions hypersensitive to  $KMnO_4$  are labelled ( $RP_0$  and  $RP_{INIT}$ ) and depicted at the bottom of the figure. The coordinates are relative to the transcription start point. Chemical sequencing reactions for purines (G + A) are shown and the relevant regions of  $P_{\omega}$  depicted to the right of the figure.

### Protein $\omega_2$ interacts with the $NH_2$ -terminal half of the $RNAP-\sigma^A$ $\beta'$ subunit

$RNAP-\sigma^A$  and  $\omega_2$  cooperatively bind  $P_{\omega}$  DNA cooperatively and create higher-order nucleoprotein complexes that reflect the combinatorial control of gene expression (Figures 2–4). This effect is likely attributed to direct protein–protein interactions between adjacent DNA-binding factors that promote the assembly of higher-order complexes. To determine whether or not  $RNAP-\sigma^A$  and  $\omega_2$  physically interacted,  $RNAP-\sigma^A$  was bound to a  $Ni^{2+}$  agarose column through coordination with the C-terminal histidine tag of its  $\beta'$  subunit (30). The  $RNAP-\sigma^A$ -bound matrix retained  $\omega_2$ , even in the absence of  $P_{\omega}$  DNA. These proteins also co-eluted from the matrix during an elution step (Supplementary Figure S6).

Initial identification of the  $RNAP-\sigma^A$  subunit(s) responsible for association to  $\omega_2$  was achieved by carrying out far-western blots of  $RNAP-\sigma^A$ ,  $\omega_2$  and BSA as control. These proteins were resolved by SDS-PAGE under conditions under which the small  $\omega$  protein (7.9 kDa) migrated with the front. After renaturation of prey proteins and a membrane blocking step, the bait,  $\omega_2$ , was added. Protein–protein interactions were detected using anti- $\omega_2$  polyclonal antibodies. As expected,  $\omega_2$  interacted with itself and also with the co-migrating  $\beta$  and/or  $\beta'$  subunits of  $RNAP-\sigma^A$ . No other

subunits gave a signal (Figure 5A). Due to a similarity in mass,  $\beta$  (133.6 kDa) and  $\beta'$  (134.2 kDa) subunits could not be distinguished. We therefore took advantage of the fact that all *B. subtilis*  $RNAP-\sigma^A$  subunits, except for  $\beta'$  (pI 8.8), have acidic pIs and repeated the far-western experiments, this time using two-dimensional (2D)-PAGE. Protein  $\omega_2$  interacted with  $\beta'$  and several proteins in unexpected spots (termed 1–2, 3–4 and 5). These had masses of  $\sim 34$  kDa and were located in the basic region of the gel (Figure 5B, Ab-anti  $\omega_2$  condition). Corresponding polypeptides were extracted from the gel, subjected to mass spectrometry analysis, and identified as  $RNAP-\sigma^A$   $\beta'$  subunit NTDs with slight variations in the C-termini (Figure 5C). Taking into account the sizes observed, it was assumed that the Sw2 structural module (residues 316–342) was missing from these NTD variants of the  $\beta'$  subunit.

### The central and C-terminal regions of $\omega_2$ appears not to interact with $RNAP-\sigma^A$

The  $\omega_2$  protein has three functional regions: (i) the unstructured NTD (residues 1–24), which is essential for the  $\omega_2 \cdot \delta_2$  interaction (11, 15); (ii) the  $\beta$ -sheet domain (residues 28–32), which is required for  $\omega_2$  recognition of its cognate DNA site (9, 14); and (iii) the  $\alpha$ -helix  $\alpha 1$  (residues 34–46) which, in concert with the  $\alpha 2$  helix (residues 51–64) contributes to

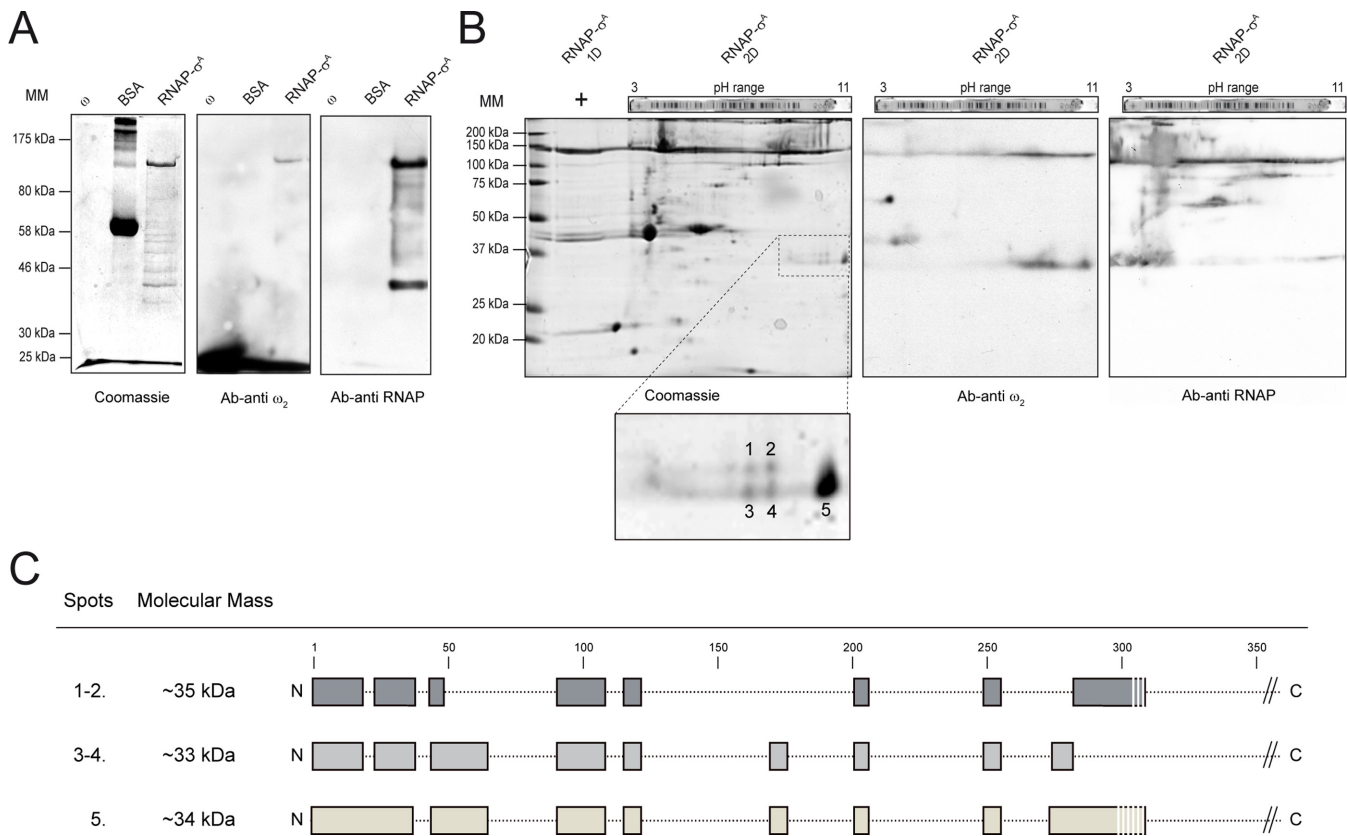


**Figure 5.** Far-western blotting of  $\omega_2$  and RNAP- $\sigma^A$ . (A) 1  $\mu$ g  $\omega_2$ , 1  $\mu$ g RNAP- $\sigma^A$  or 5  $\mu$ g BSA (as control) were resolved by SDS-PAGE and either stained with Coomassie blue or transferred onto nitrocellulose membranes. Membranes underwent a renaturing step and incubated with the specific  $\omega_2$  and RNAP- $\sigma^A$  antibodies (Ab). (B) 1  $\mu$ g RNAP- $\sigma^A$  was resolved by iso-electric focusing in a pH 3–11 gradient followed by an SDS-PAGE. Protein was then transferred to a membrane, renatured, incubated with the  $\omega_2$  bait and highlighted with either Ab-anti  $\omega_2$  or Ab-anti RNAP- $\sigma^A$ . (C) Basic, ~34 kDa polypeptides (1–5) that had reacted with Ab-anti  $\omega_2$  were gel purified and identified by mass spectrometry. The regions identified are shown in this figure. The sequence coverage was > 40%.

monomer-monomer and dimer-dimer interfaces (8,9). The function, if any, of the C-terminal region (residues 65–71) is unknown (7,8).

Significantly, the 79-residue long  $\omega_2$  (9.0 kDa) shares a 98% identity with the 71-residue  $\omega$  for the first 55 residues (Supplemental material Annex 2). However, they only share an 18% identity in the last 24 residues (Supplementary Figure S7A). The  $\omega_2$  protein repressed  $P_\delta$  utilization *in vivo* nearly as efficiently as wt  $\omega_2$  (Supplemental material Annex 2, Supplementary Figure S7B). Similar results were observed when the  $P_\delta$ -*lacZ* fusion was replaced by the  $P_\omega$ -*lacZ* fusion (data not shown). Furthermore, plasmid-borne  $\omega_2$  and  $\delta$  genes which were transcribed from  $P_\omega$  (*parS2*) and  $P_\delta$  (*parS1*) (Figure 1A), were necessary and sufficient for stabilizing of an otherwise unstable plasmid in *B. subtilis* cells (38, our unpublished results). It is likely that: (i) the dimer is the functional unit of  $\omega_2$ ; (ii)  $\omega_2$  interacts with  $\delta_2$  just like  $\omega$ ; and (iii) the different C-terminal domains of  $\omega$  and  $\omega_2$  are not involved in gene repression.

Protein docking experiments predicted that the unstructured  $\omega$  NTD folded into an  $\alpha$ -helical structure that interacted with the  $\beta'$  NTD of RNAP- $\sigma^A$  (Supplementary Figure S8). In contrast, several charged amino acids located in the coiled region between the  $\alpha$ -helices  $\alpha 1$  and  $\alpha 2$  (residues 47–52) and in the  $\alpha 2$  helix itself (residues 51–64) could make

contacts with the oppositely charged residues in the  $\beta'$  sub-unit of RNAP- $\sigma^A$ . To test this hypothesis (Supplemental material Annex 3), the charged residues that were accessible in these domains, K52, E53, D56, R64 and K70, were replaced with alanine. Subsequently, the *in vivo* behaviour of these mutants was investigated (Supplemental material Annex 3). With the exception of  $\omega$ D56A, the  $\omega$  mutant variants repressed  $P_\delta$  transcription *in vivo* as efficiently as wt  $\omega_2$  (Supplementary Figure S7B) (Supplemental material Annex 3). The D56A mutant only reduced  $P_\delta$  transcription ~6-fold. As described in Supplementary Annex 3, purified  $\omega$ D56A also formed dimers, albeit in a far smaller proportion than wt  $\omega_2$  (Supplementary Figure S7C). Since in the dimeric form of  $\omega$ , the  $\beta$ -sheet domain adopts an antiparallel configuration before binding  $P_\omega$ , the primary defect of  $\omega$ D56A might be a poor ability to dimerize. Therefore, it was not further analysed. It would be very interesting to determine whether or not the  $\omega_2$  NTD can, by itself recruit RNAP- $\sigma^A$  to the  $\omega_2$ - $P_\omega$  DNA complex.

## DISCUSSION

Direct contacts between  $\omega_2$  and RNAP- $\sigma^A$  stimulate RP<sub>C</sub> complex formation and its subsequent isomerization to RP<sub>O</sub>. This appears to be the mechanism by which limiting

concentrations of  $\omega_2$  activate  $P_\omega$  transcription. This process is further enhanced by  $\delta_2$  (Figure 3B). However, stoichiometric concentrations of  $\omega_2$  have the opposite effect: here the recruited RNAP- $\sigma^A$  inefficiently isomerizes into  $RP_O$  and represses  $P_\omega$  or  $P_\delta$  transcription both *in vivo* and *in vitro*. It would be highly interesting to determine whether or not  $\omega_2$  functions as an activator to repressor switch of  $P_{copS}$ . However, preliminary results indicate that  $\omega_2 \cdot P_{copS}$  DNA forms a ternary complex with RNAP- $\sigma^A$  and that  $\omega_2$  regulates transcription through a mechanism that does not exclude the RNAP- $\sigma^A$  from the  $RP_C$  (4).

### The dual activity of the $\omega_2$ regulator

Plasmid-encoded  $\omega_2$ , from Gram-positive cocci, is the only one out of the more than 2000 RHH<sub>2</sub> proteins that can either activate or repress the utilization of a single promoter ( $P_\omega$ ) in a concentration-dependent manner. This is true at least in a simplified *in vitro* system. The majority of RHH<sub>2</sub> proteins are predicted to be transcriptional repressors (39). However, four of them act both as activators and as repressors. These are: a P22-Arc variant, Mer, AmrZ [AlgZ] and NikR. They bind to a variety of promoters, functioning as repressors for some while behaving as activators for others (40–43). In the case of other putative regulators, various metal cofactors and different stoichiometries might also influence the effect they have on promoter functioning (40–43).

The activator to repressor switch function of  $\omega_2$  appears to be managed by the diverse modes of  $\omega_2$  binding to the operator region of  $P_\omega$ . These modes of binding have distinct effects on the initial activity of RNAP- $\sigma^A$ . Under limiting concentrations,  $\omega_2$  promotes RNAP- $\sigma^A$  binding to operator sequences that overlap the  $-35$  sequence. This results in the stimulation of  $RP_C$  formation and in an increase in the rate of isomerization from  $RP_C$  to  $RP_O$ . It is thus likely that: (i)  $\omega_2$  increases the local concentration of both proteins, leading to a ternary  $\omega_2 \cdot P_\omega \cdot$  RNAP- $\sigma^A$  complex; (ii) this ternary complex facilitates the rate of isomerization from  $RP_C$  to  $RP_O$  and increases  $P_\omega$  dependent mRNA synthesis; and (iii)  $\delta_2$  may act as a co-activator by increasing the half-life of  $\omega_2 \cdot P_\omega$  DNA complexes (see 13).

With stoichiometric concentrations of  $\omega_2$  full operator occupancy was achieved, and a different outcome was observed. Under these conditions,  $\omega_2$  assembles into a left-handed matrix that wraps around right-handed, straight  $P_\omega$  DNA (see Figure 1B). This assembly makes  $P_\omega$  DNA accessible to RNAP- $\sigma^A$  ( $RP_C$  formation), while simultaneously inhibiting isomerization to  $RP_O$  (transcriptional repression) (Figure 4, lanes 17–18). *In vitro*, we observed that  $\delta_2$  contributed to  $P_\delta$  repression (Figure 3B), and the presence of both  $\omega_2$  and  $\delta_2$  transcriptional repression of  $P_\delta$  and  $P_\omega$  was elevated *in vivo* with respect to wt  $\omega_2$  alone (Supplementary Figure S7B, data not shown). When stoichiometric concentrations of  $\omega_2$  were added to preformed  $RP_O$  complexes, a moderate effect on  $P_\omega$  utilization was observed (see Figures 3 and 4). This suggested that RNAP- $\sigma^A$  transcription was influenced by  $\omega_2$  that was bound to its cognate promoters. In sum, we describe here a previously uncharacterized mechanism of transcription regulation in bacteria belonging to the phylum Firmicutes.

Several different models can be considered in order to explain the specific transcriptional repression resulting from the full occupancy of the operator sequences by  $\omega_2$ : (i) relocation of RNAP- $\sigma^A$  to a position unfavourable for efficient  $RP_O$  formation; (ii) 'locking' RNAP- $\sigma^A$  into a conformation unfavourable for  $RP_O$  formation; (iii) blocking the interaction between the  $\beta'$  NTD and the DNA, which may be an essential step for  $RP_O$  formation; and (iv) inhibition of RNAP- $\sigma^A$  mediated transcription by hindering any putative upstream element. We favour the first model because  $RP_C$  formation is stimulated by the interaction between  $\omega_2$  and RNAP- $\sigma^A$ , while the subsequent isomerization step producing stable  $RP_O$  (through the unstable intermediate,  $RP_I$ ) becomes inhibited. Also consistent with this model is the fact that  $\omega_2$  establishes interactions with operator sites when RNAP- $\sigma^A$  is already bound to  $P_\omega$  DNA. Meanwhile,  $\omega_2$  fails to inhibit pre-formed  $RP_O$ . Also in line with this model is the observation that, in the presence of limiting amounts of  $\omega_2$  bound to  $P_\omega$  DNA, RNAP- $\sigma^A$  moves onto  $P_\omega$  DNA (Supplementary Figure S2A), and that while under saturating concentrations of  $\omega_2$ , RNAP- $\sigma^A$  moves off of  $P_\omega$  DNA (Supplementary Figure S2B).

### The interplay between the $\omega_2$ regulator and the $\beta'$ subunit of RNAP holoenzyme

The work presented here establishes that  $\omega_2$  is a global regulator of plasmid biology through its effect on replication, faithful partitioning and better-than random segregation (see Introduction). Importantly,  $\omega_2$  represents an exception to the accepted prokaryotic transcription regulation paradigm, which asserts that, there are proteins that can act as either activators or repressors, but that the same protein cannot act as both. Since  $\omega_2$  regulates the expression of plasmid encoded genes that are harboured in different Firmicutes bacteria, it presumably recognizes the RNAP  $\beta'$  NTD of all of them. This recognition might be limited to the first 316 amino acids, the length of the shortest polypeptide of the  $\beta'$  subunit that binds  $\omega_2$  (Figure 5B). This would not be surprising because the  $\beta'$  subunits of all Firmicutes share a high degree of sequence identity. Consistent with this,  $\omega_2$  does not regulate transcription of a genetically distant bacterium (e.g. *E. coli*) (16). These facts imply that the regions of the Firmicutes  $\beta'$  subunits that show a significant degree of sequence divergence are not involved in  $\omega_2$  binding, such as residues 124–165 and 178–208 (22% and 13%, respectively). Presumably, residues 260–271, which match almost perfectly between the  $\beta'$  subunits of *E. coli* and *B. subtilis*, is a region also not involved in  $\omega_2$  binding.

Few proteins have been observed to interact with the RNAP  $\beta'$  subunit. Most of these are encoded by proteobacterial phages. The phage Xp10-p7 factor interacts with the first 10 residues of the NTD of  $\beta'$  (44). The Mu-C protein binds to part of region F (b7) (45). T7-Gp2 recognizes part of the jaw (b9-b10) and  $\sigma$  1.1 domains (46,47). And lastly, N4-SSB interacts with part of region H (b11) at the CTD (48). These regulators do not share a specific target domain and have different modes of action: N4-SSB and Mu-C specifically act as transcription activators (45,48), while T7-Gp2 and Xp10-p7 are repressors (44,46). In contrast,  $\omega_2$  has a dual function (Figure 3B). Of these regulators,

only T7-Gp2, Xp10-p7, and  $\omega_2$  act during the early stages of RNAP- $\sigma$  isomerization. Meanwhile, T7-Gp2 and Xp10-p7 directly interact with RNAP- $\sigma$  rather than binding to *P* DNA as does  $\omega_2$  (44,46,47).

### Biological implication of $\omega_2$ -mediated transcription regulation

A growing number of plasmid-encoded genetic determinants for resistance to diverse antimicrobials among streptococci, enterococci and staphylococci has been shown to be regulated by  $\omega$ -like cofactors. They act either as part of the  $\omega\epsilon\zeta$  operon or on their own as part of the  $\omega$  cassette ( $\omega$  or  $\omega_2$  genes) (1). In conjunction with  $\delta_2$  and RNAP- $\sigma$ , the biological role of  $\omega_2$  as a dual regulator is to control vital plasmid functions in Firmicutes. It corrects the downward fluctuations in plasmid copy number through regulation of the synthesis of CopS (also termed CopF, CopR). CopS is a repressor of the initiator RepS (also termed RepE, RepR) protein.  $\omega_2$  also controls the synthesis of the toxin-antitoxin module, which in turn restricts the survival of plasmid-free segregants. The  $\omega_2$  protein mediates the synthesis of the partition system by regulating the expression of  $\delta_2$  and  $\omega_2$ . Protein  $\omega_2$  manages the expression of the *ermB* gene (4,16,49). With the help of  $\delta_2$  (the ParA ATPase), the  $\omega_2$  (the ParB centromere binding) protein also safeguards plasmid faithful segregation via the ParAB system. The regulation of Firmicutes RNAP- $\sigma^A$  by the  $\omega$  cassette is a newly characterized mechanism through which bacterial transcription of a large number of antibiotic resistance genes is regulated.

### SUPPLEMENTARY DATA

Supplementary Data are available at NAR Online.

### ACKNOWLEDGEMENT

We thank Margarita Salas and José M Lazaro for their generous gift of rabbit polyclonal anti-RNAP- $\sigma^A$ . This work was supported in part by grant BFU2012–39879-C02-01 awarded to J.C.A by the Dirección General de Investigación-Ministerio de Economía y Competitividad (DGI-MINECO). A.V. thanks the Consejería de Educación de la Comunidad de Madrid for its fellowship (CPI/0266/2008) and the European Social Fund (ESF). M.T. is a PhD fellow supported by the La Caixa Foundation International Fellowship Programme of La Caixa/CNB.

### FUNDING

Funding for open access charge: Dirección General de Investigación-Ministerio de Economía y Competitividad [BFU2012-39879-C02-01 to J.C.A.].

Conflict of interest statement. None declared.

### REFERENCES

- Volante, A., Soberón, N.E., Ayora, S. and Alonso, J.C. (2014) The interplay between different stability systems contributes to faithful segregation: *Streptococcus pyogenes* pSM19035 as a model. *Microbiol. Spectrum*, **2**, PLAS-0007.

- Croucher, N.J., Harris, S.R., Fraser, C., Quail, M.A., Burton, J., van der Linden, M., McGee, L., von Gottberg, A., Song, J.H., Ko, K.S. *et al.* (2011) Rapid pneumococcal evolution in response to clinical interventions. *Science*, **331**, 430–434.
- Camacho, A.G., Misselwitz, R., Behlke, J., Ayora, S., Welfle, K., Meinhart, A., Lara, B., Saenger, W., Welfle, H. and Alonso, J.C. (2002) *In vitro* and *in vivo* stability of the  $\epsilon_2\zeta_2$  protein complex of the broad host-range *Streptococcus pyogenes* pSM19035 addiction system. *Biol. Chem.*, **383**, 1701–1713.
- de la Hoz, A.B., Ayora, S., Sitkiewicz, I., Fernandez, S., Pankiewicz, R., Alonso, J.C. and Ceglowski, P. (2000) Plasmid copy-number control and better-than-random segregation genes of pSM19035 share a common regulator. *Proc. Natl. Acad. Sci. U.S.A.*, **97**, 728–733.
- Dmowski, M., Sitkiewicz, I. and Ceglowski, P. (2006) Characterization of a novel partition system encoded by the  $\delta$  and  $\omega$  genes from the streptococcal plasmid pSM19035. *J. Bacteriol.*, **188**, 4362–4372.
- Liyo, V.S., Pratto, F., de la Hoz, A.B., Ayora, S. and Alonso, J.C. (2010) Plasmid pSM19035, a model to study stable maintenance in Firmicutes. *Plasmid*, **64**, 1–17.
- Murayama, K., de la Hoz, A.B., Alings, C., Lopez, G., Orth, P., Alonso, J.C. and Saenger, W. (1999) Crystallization and preliminary X-ray diffraction studies of *Streptococcus pyogenes* plasmid pSM19035-encoded  $\omega$  transcriptional repressor. *Acta Crystallogr. D Biol. Crystallogr.*, **55**, 2041–2042.
- Murayama, K., Orth, P., de la Hoz, A.B., Alonso, J.C. and Saenger, W. (2001) Crystal structure of  $\omega$  transcriptional repressor encoded by *Streptococcus pyogenes* plasmid pSM19035 at 1.5 Å resolution. *J. Mol. Biol.*, **314**, 789–796.
- Weihofen, W.A., Cicek, A., Pratto, F., Alonso, J.C. and Saenger, W. (2006) Structures of  $\omega$  repressors bound to direct and inverted DNA repeats explain modulation of transcription. *Nucleic Acids Res.*, **34**, 1450–1458.
- de la Hoz, A.B., Pratto, F., Misselwitz, R., Speck, C., Weihofen, W., Welfle, K., Saenger, W., Welfle, H. and Alonso, J.C. (2004) Recognition of DNA by  $\omega$  protein from the broad-host range *Streptococcus pyogenes* plasmid pSM19035: analysis of binding to operator DNA with one to four heptad repeats. *Nucleic Acids Res.*, **32**, 3136–3147.
- Welfle, K., Pratto, F., Misselwitz, R., Behlke, J., Alonso, J.C. and Welfle, H. (2005) Role of the N-terminal region and of  $\beta$ -sheet residue Thr29 on the activity of the  $\omega_2$  global regulator from the broad-host range *Streptococcus pyogenes* plasmid pSM19035. *Biol. Chem.*, **386**, 881–894.
- Pratto, F., Suzuki, Y., Takeyasu, K. and Alonso, J.C. (2009) Single-molecule analysis of protein-DNA complexes formed during partition of newly replicated plasmid molecules in *Streptococcus pyogenes*. *J. Biol. Chem.*, **284**, 30298–30306.
- Soberón, N.E., Liyo, V.S., Pratto, F., Volante, A. and Alonso, J.C. (2011) Molecular anatomy of the *Streptococcus pyogenes* pSM19035 partition and segrosome complexes. *Nucleic Acids Res.*, **39**, 2624–2637.
- Dostál, L., Pratto, F., Alonso, J.C. and Welfle, H. (2007) Binding of regulatory protein  $\omega$  from *Streptococcus pyogenes* plasmid pSM19035 to direct and inverted 7-Base pair repeats of operator DNA. *J. Raman Spectrosc.*, **38**, 166–175.
- Volante, A. and Alonso, J.C. (2015) Molecular anatomy of ParA-ParA and ParA-ParB interactions during plasmid partitioning. *J. Biol. Chem.*, **290**, 18782–18795.
- Pratto, F., Cicek, A., Weihofen, W.A., Lurz, R., Saenger, W. and Alonso, J.C. (2008) *Streptococcus pyogenes* pSM19035 requires dynamic assembly of ATP-bound ParA and ParB on parS DNA during plasmid segregation. *Nucleic Acids Res.*, **36**, 3676–3689.
- Record, M. Jr, Reznikoff, W., Craig, M., McQuade, K. and Schlax, P. (1996) In: Neidhardt, F., Curtiss, R.I., Ingraham, J., Lin, E., Low, K., Magasanik, B., Reznikoff, W., Riley, M., Schaechter, M. and Umberger, H. (eds). *In Escherichia coli and Salmonella: Cellular and Molecular Biology*. 2nd Edn. ASM Press, Washington, DC, pp. 792–821.
- Vassilyev, D.G., Vassilyeva, M.N., Perederina, A., Tahirov, T.H. and Artsimovitch, I. (2007) Structural basis for transcription elongation by bacterial RNA polymerase. *Nature*, **448**, 157–162.
- Lane, W.J. and Darst, S.A. (2010) Molecular evolution of multisubunit RNA polymerases: structural analysis. *J. Mol. Biol.*, **395**, 686–704.

20. Zhang, Y., Feng, Y., Chatterjee, S., Tuske, S., Ho, M.X., Arnold, E. and Ebright, R.H. (2012) Structural basis of transcription initiation. *Science*, **338**, 1076–1080.
21. Darst, S.A. (2001) Bacterial RNA polymerase. *Curr. Opin. Struct. Biol.*, **11**, 155–162.
22. Murakami, K.S. and Darst, S.A. (2003) Bacterial RNA polymerases: the whole story. *Curr. Opin. Struct. Biol.*, **13**, 31–39.
23. Gruber, T.M. and Gross, C.A. (2003) Multiple  $\sigma$  subunits and the partitioning of bacterial transcription space. *Annu. Rev. Microbiol.*, **57**, 441–466.
24. Ebright, R.H. (2000) RNA polymerase: structural similarities between bacterial RNA polymerase and eukaryotic RNA polymerase II. *J. Mol. Biol.*, **304**, 687–698.
25. Haugen, S.P., Ross, W. and Gourse, R.L. (2008) Advances in bacterial promoter recognition and its control by factors that do not bind DNA. *Nat. Rev. Microbiol.*, **6**, 507–519.
26. Murakami, K.S., Masuda, S., Campbell, E.A., Muzzin, O. and Darst, S.A. (2002) Structural basis of transcription initiation: an RNA polymerase holoenzyme-DNA complex. *Science*, **296**, 1285–1290.
27. Vassylyev, D.G., Sekine, S., Laptenko, O., Lee, J., Vassylyeva, M.N., Borukhov, S. and Yokoyama, S. (2002) Crystal structure of a bacterial RNA polymerase holoenzyme at 2.6 Å resolution. *Nature*, **417**, 712–719.
28. Saecker, R.M., Record, M.T. Jr and Dehaseth, P.L. (2011) Mechanism of bacterial transcription initiation: RNA polymerase - promoter binding, isomerization to initiation-competent open complexes, and initiation of RNA synthesis. *J. Mol. Biol.*, **412**, 754–771.
29. Browning, D.F. and Busby, S.J. (2004) The regulation of bacterial transcription initiation. *Nat. Rev. Microbiol.*, **2**, 57–65.
30. Fujita, M. and Sadaie, Y. (1998) Rapid isolation of RNA polymerase from sporulating cells of *Bacillus subtilis*. *Gene*, **221**, 185–190.
31. Miller, J.H. (1972) *Experiments in Molecular Genetics*, Cold Spring Harbor Lab. Press, Plainview, NY.
32. Zechel, K. (1977) On the resolution of polypeptides by isoelectric focusing in polyacrylamide gels in the presence of urea and nonidet-p40. *Anal. Biochem.*, **83**, 240–251.
33. Wu, Y., Li, Q. and Chen, X.Z. (2007) Detecting protein-protein interactions by Far western blotting. *Nat. Protoc.*, **2**, 3278–3284.
34. Lioy, V.S., Martin, M.T., Camacho, A.G., Lurz, R., Antelmann, H., Hecker, M., Hitchin, E., Ridge, Y., Wells, J.M. and Alonso, J.C. (2006) pSM19035-encoded  $\zeta$  toxin induces stasis followed by death in a subpopulation of cells. *Microbiology*, **152**, 2365–2379.
35. Tapias, A., Fernandez, S., Alonso, J.C. and Barbe, J. (2002) *Rhodobacter sphaeroides* LexA has dual activity: optimising and repressing *recA* gene transcription. *Nucleic Acids Res.*, **30**, 1539–1546.
36. Rodionov, O., Lobočka, M. and Yarmolinsky, M. (1999) Silencing of genes flanking the P1 plasmid centromere. *Science*, **283**, 546–549.
37. Lynch, A.S. and Wang, J.C. (1995) SopB protein-mediated silencing of genes linked to the *sopC* locus of *Escherichia coli* F plasmid. *Proc. Natl. Acad. Sci. U.S.A.*, **92**, 1896–1900.
38. Lioy, V.S., Volante, A., Soberón, N.E., Lurz, R., Ayora, S. and Alonso, J.C. (2015) ParAB partition dynamics in Firmicutes: nucleoid bound ParA captures and tethers ParB-plasmid complexes. *PLoS One*, **10**, e0131943 .
39. Schreiter, E.R. and Drennan, C.L. (2007) Ribbon-helix-helix transcription factors: variations on a theme. *Nat. Rev. Microbiol.*, **5**, 710–720.
40. Smith, T.L. and Sauer, R.T. (1996) Dual regulation of open-complex formation and promoter clearance by Arc explains a novel repressor to activator switch. *Proc. Natl. Acad. Sci. U.S.A.*, **93**, 8868–8872.
41. Schreiter, E.R., Sintchak, M.D., Guo, Y., Chivers, P.T., Sauer, R.T. and Drennan, C.L. (2003) Crystal structure of the nickel-responsive transcription factor NikR. *Nat. Struct. Biol.*, **10**, 794–799.
42. Muller, C., Bahlawane, C., Aubert, S., Delay, C.M., Schauer, K., Michaud-Soret, I. and De Reuse, H. (2011) Hierarchical regulation of the NikR-mediated nickel response in *Helicobacter pylori*. *Nucleic Acids Res.*, **39**, 7564–7575.
43. Pryor, E.E. Jr, Waligora, E.A., Xu, B., Dellos-Nolan, S., Wozniak, D.J. and Hollis, T. (2012) The transcription factor AmrZ utilizes multiple DNA binding modes to recognize activator and repressor sequences of *Pseudomonas aeruginosa* virulence genes. *PLoS Pathog.*, **8**, e1002648.
44. Yuzenkova, Y., Zenkin, N. and Severinov, K. (2008) Mapping of RNA polymerase residues that interact with bacteriophage Xp10 transcription antitermination factor p7. *J. Mol. Biol.*, **375**, 29–35.
45. Swapna, G., Chakraborty, A., Kumari, V., Sen, R. and Nagaraja, V. (2011) Mutations in beta' subunit of *Escherichia coli* RNA polymerase perturb the activator polymerase functional interaction required for promoter clearance. *Mol. Microbiol.*, **80**, 1169–1185.
46. James, E., Liu, M., Sheppard, C., Mekler, V., Camara, B., Liu, B., Simpson, P., Cota, E., Severinov, K., Matthews, S. et al. (2012) Structural and mechanistic basis for the inhibition of *Escherichia coli* RNA polymerase by T7 Gp2. *Mol. Cell*, **47**, 755–766.
47. Bae, B., Davis, E., Brown, D., Campbell, E.A., Wigneshweraraj, S. and Darst, S.A. (2013) Phage T7 Gp2 inhibition of *Escherichia coli* RNA polymerase involves misappropriation of  $\sigma^{70}$  domain 1.1. *Proc. Natl. Acad. Sci. U.S.A.*, **110**, 19772–19777.
48. Miller, A., Wood, D., Ebright, R.H. and Rothman-Denes, L.B. (1997) RNA polymerase beta' subunit: a target of DNA binding-independent activation. *Science*, **275**, 1655–1657.
49. Lioy, V.S., Machon, C., Tabone, M., Gonzalez-Pastor, J.E., Daugelavicius, R., Ayora, S. and Alonso, J.C. (2012) The  $\zeta$  toxin induces a set of protective responses and dormancy. *PLoS One*, **7**, e30282.